Improving the accuracy of Weyl-Heisenberg wavelet and symmetrized Gaussian representations using customized phase-space-region operators

Richard Lombardini and Bill Poirier*
Department of Chemistry and Biochemistry, and Department of Physics, Texas Tech University, P.O. Box 41061, Lubbock, Texas 79409-1061, USA
(Received 22 June 2006; published 26 September 2006)

A particular basis set method developed by one of the authors, involving maximally localized orthogonal Weyl-Heisenberg wavelets (or "weylets") and a phase space truncation scheme, has been successfully applied to exact quantum calculations for many degrees of freedom (DOF's) [B. Poirier and A. Salam, J. Chem. Phys. **121**, 1740 (2004)]. However, limitations in accuracy arise in the many-DOF case, owing to memory limits on conventional computers. This paper addresses this accuracy limitation by introducing phase space region operators (PSRO's) that customize individual weylet basis functions for the problem of interest. The construction of the PSRO's is straightforward, and does not require *a priori* knowledge of the desired eigenstates. The PSRO, when applied to weylets, as well as to simple phase space Gaussian basis functions, exhibits remarkable improvements in accuracy, reducing computed eigenvalue errors by orders of magnitude. The method is applied to various model systems at varying DOF's.

DOI: 10.1103/PhysRevE.74.036705 PACS number(s): 02.70.−c, 05.45.Mt, 31.15.Qg

I. INTRODUCTION

For molecular bound state calculations, the choice of basis directly determines the computational effort in solving the quantum Hamiltonian. More specifically, the efficiency K/N, where N represents the number of basis functions needed to calculate K eigenvalues at a desired accuracy, has a strong dependence on the degree of correlation between the basis functions and the target system. This relationship has prompted research in basis optimization which focuses on the maximization of the efficiency and thus, ultimately, the reduction of CPU effort and memory usage.

Symmetrized Weyl-Heisenberg wavelets, or "weylets," comprise a type of universal orthonormal basis that can be effectively used to represent any bound molecular system with an efficiency approaching perfection ($K/N \to 1$) in the large N and K limit, regardless of system dimensionality. Although the weylet basis functions themselves are universal, the truncation of the basis set, achieved using a phase space truncation scheme [1–3], is what tailors the method to individual systems. In contrast, all direct product basis sets (DPB's) [4,5], even those for which individual basis functions are optimized via self-consistent field or other techniques [6–9], exhibit exponential reduction in efficiency with f, the number of degrees of freedom (DOF's) [9,10]. Consequently, the weylet approach has been applied to direct matrix eigenvalue calculations for model systems of 15 DOF's and beyond [3], far beyond what would be feasible using a DPB. Recently, the method was successfully applied to a real molecular system Ne_2 (in Cartesian coordinates) [11]. Although Ne_2 presents a "worst-case scenario" for the weylet method, in that f and K are small, and includes states near the dissociation threshold, it is still competitive with other state-of-the-art exact quantum dynamics methods [12].

Phase space truncation of the weylet basis is effective because individual weylet functions have good phase space localization and are orthogonal. Achieving both properties together is nontrivial [13,14], but can be achieved using a momentum-symmetrization modification first introduced by Wilson [15] and Daubechies *et al.* [16]. In 1 DOF, one starts with a $2\times$ overcomplete set of coherent states (CS's) which are derived from phase space Gaussians and arranged on a doubly dense lattice (i.e., two CS's per Planck cell) on phase space. Provided the lattice of CS's constitutes a tight frame, a particular linear combination of positive and negative momentum CS pairs then yields a complete 1 DOF orthonormal weylet basis $|\varphi_i\rangle$ (the general f DOF case is addressed in Sec. II A). Poirier [1–3] later refined the approach by constructing maximally phase space localized weylets, in a computationally tractable manner for quantum dynamics calculations.

To understand phase space truncation, we must first introduce two projection operators

$$\hat{\rho}_N = \sum_{i=1}^{N} |\varphi_i\rangle\langle\varphi_i| \tag{1}$$

and

$$\hat{\rho}_K = \Theta[E_{\max} - \hat{H}(\hat{q},\hat{p})]. \tag{2}$$

The Wigner-Weyl phase space representation [17–20] of $\hat{\rho}_K$ (simply labeled as "ρ_K") [see Fig. 1(a)] is a function that oscillates about unity in the classically allowed region (QC, for "quasiclassical") of phase space where $H \leq E_{\max}$, and is damped exponentially outside this region. It can be shown that

$$\rho_K \approx \rho_K^{\mathrm{QC}} = \Theta[E_{\max} - H(q,p)] \tag{3}$$

in the large K limit, i.e., ρ_K can be associated with the classically allowed region of phase space $\mathcal{R}$ [21].

Similarly, each single DOF weylet $|\varphi_i\rangle$ can be associated with a (momentum-symmetrized) pair of blocks (corresponding to the CS pairs mentioned ealier), centered on the lattice

*Electronic address: bill.poirier@ttu.edu

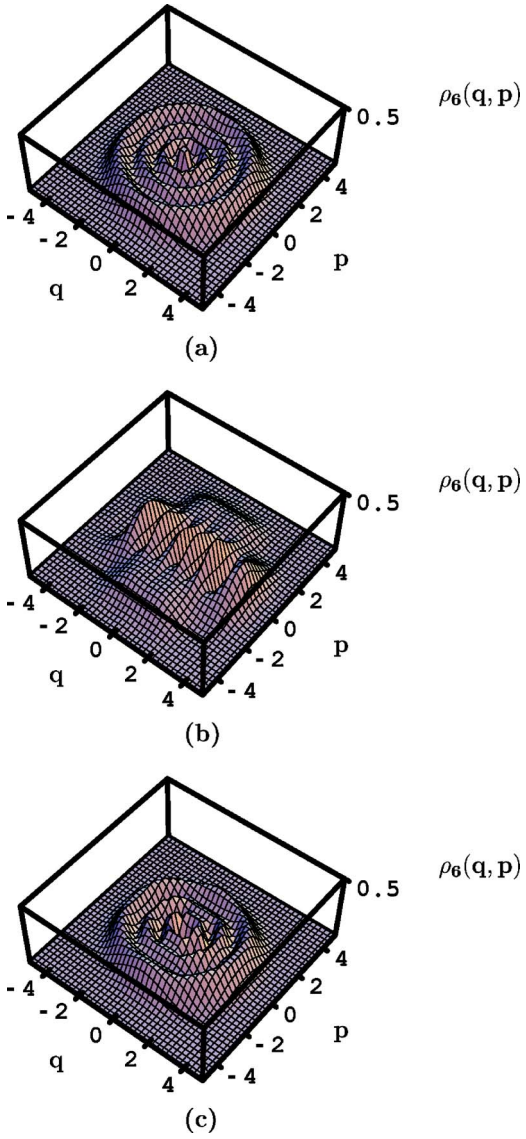

FIG. 1. (Color online) Wigner-Weyl representation (1 DOF case) of projection operators consisting of three different sets of $N=6$ (a) HO eigenstates, (b) weylets, (c) PSRO-modified weylets. Different than what is stated in Sec. I, all plots oscillate about $(1/2\pi)$ instead of unity, due to a discrepant normalization. In part (b), there are quantum interference fringes that emerge from the momentum symmetrization. The modified weylets in part (c) adopt the ringlike pattern of the true HO eigenstates, rendering them a more efficient basis for representing the HO system (see Table III).

sites, which on truncation, comprise a region $\mathcal{R}'$ [see Fig. 2(a)]. If the block size is small (i.e., N and K large), then $\mathcal{R}'$ closely resembles $\mathcal{R}$ and $N \approx K$, as the region volumes are proportional to basis size. In any event, it is the blocks in the boundary of $\mathcal{R}'$ that are the leading cause of inefficiency, since they overlap $\mathcal{R}$ only partially. This effect is more pronounced at larger dimensionalities for a given K value, so that in practice, the limiting difficulty of the weylet method is the level of computed accuracy that can be achieved, rather than dimensionality *per se*.

The main purpose of this paper is to address this limitation by customizing the individual weylet functions (i.e., not

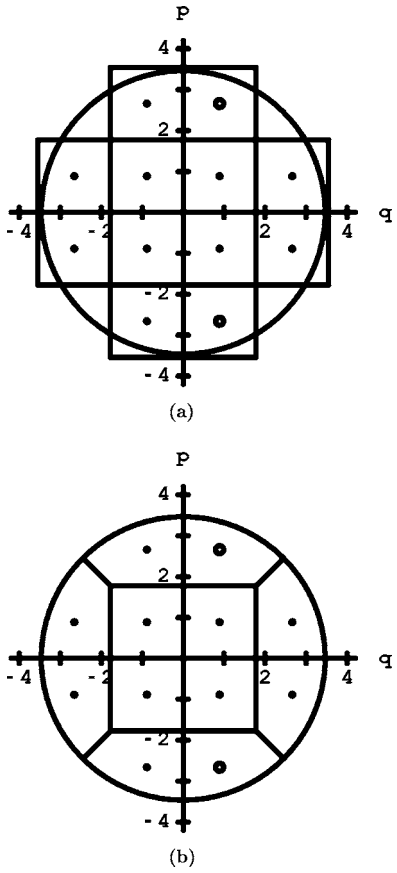

FIG. 2. Classically allowed (QC) region for the weylets and HO PSRO in the 1 DOF case in units where $a=\hbar=1$. The basis truncation criterion $H(q_s,p_t) \leq E_{\text{cut}}=4.0$ gives the weylet basis of $N=6$ functions (Table III). In part (a), the QC region of each weylet is represented by two squares each with volume π symmetrically placed about the q axis. The two squares with small unfilled circles represent the weylet $|\varphi_{1/2,3/2}\rangle$. The larger circle is the QC region $\mathcal{R}$ corresponding to the PSRO $\hat{\rho}_K^{\text{QC}}$ $(K=N=6)$. The same weylets modified by the exact projection $\hat{\rho}_K$ are approximately given in part (b).

just their truncation) for particular applications. Consider that the basis $\hat{\rho}_K|\varphi_i\rangle=|\varphi_i'\rangle$, rather than $|\varphi_i\rangle$ itself, can in principle result in an exact calculation of the lowest K eigenvalues. In the phase space picture, this projection effectively transforms Fig. 2(a) to Fig. 2(b) which is seen to yield $\mathcal{R}=\mathcal{R}'$ even when N and K are not large. Note that the peripheral basis functions are most affected by the projection transformation.

In practice, the above picture is complicated by additional concerns. First, the $|\varphi_i'\rangle$ are not orthogonal—though this is easily remedied via orthogonalization [22] or direct solution of the generalized eigenvalue problem

$$\tilde{H}\vec{v} = E\tilde{S}\vec{v}, \tag{4}$$

where $\tilde{H}$ and $\tilde{S}$ are the Hamiltonian and overlap matrices, respectively, in the nonorthogonal basis representation, and $(E,\vec{v})$ is the (eigenvalue,eigenvector) pair. More importantly, $|\varphi_i'\rangle$ might in principle be linearly *dependent* or nearly so,

and in fact this is almost certain to cause numerical instabilities if $|\varphi_i\rangle$ is a "random" basis or even DPB, at sufficiently large f or N. Use of phase space truncated weylets as the starting basis, $|\varphi_i\rangle$, almost completely alleviates this difficulty, however. Finally, $\hat{\rho}_K$ is not known *a priori*—though $\hat{\rho}_K^{\mathrm{QC}}$ *is* known, and is likely to constitute a worthy substitute. Fortunately, the mathematical development of $\hat{\rho}_K^{\mathrm{QC}}$, or what we call the "phase space region operator" (PSRO), and its action on arbitrary functions, has been extensively studied by Bracken, Doebner, and Wood [23,24]. With their insights, we have developed very efficient projected basis sets, $\hat{\rho}_K^{\mathrm{QC}}|\varphi_i\rangle = |\varphi_i^{(1)}\rangle$ [the "(1)" superscript will be explained later], which are shown to *greatly* increase the accuracy levels that can be obtained in weylet calculations.

A second idea explained in this paper involves the use of momentum-symmetrized Gaussians (SG's), $|\psi_i\rangle$, rather than weylets, $|\varphi_i\rangle$, as the initial basis. SG's centered on the same lattice sites as their weylet counterparts span nearly the same subspace, and individual SG's are nearly orthogonal due to the momentum symmetrization [1–3,25]. Moreover, the PSRO projected subspace of the SG's and weylets are much closer still, as compared to the unprojected case. Although $|\varphi_i^{(1)}\rangle$ is still anticipated to be more efficient than $|\psi_i^{(1)}\rangle$, the latter are far more convenient to work with numerically.

Our results indicate impressive improvements in efficiency for PSRO-modified weylets $|\varphi_i^{(1)}\rangle$, and SG's, $|\psi_i^{(1)}\rangle$, on a wide range of model systems and dimensionalities. The most noticeable improvements are in cases where N and K are small, as expected. Moreover, the efficiencies of the two projected basis sets are nearly the same, with SG's actually more efficient than weylets in some cases, making them a competitive basis if one can develop inexpensive techniques for the PSRO modification. We have also found that multiple applications of the PSRO results in further increases in efficiency for both basis sets, up to a point. The rationale here is that higher powers of $\hat{\rho}_K^{\mathrm{QC}}$ are more nearly idempotent, and therefore presumably closer to the exact projection operator $\hat{\rho}_K$.

The remainder of this paper is organized as follows. The next section presents a brief description of the weylets and SG's in the single and general f DOF cases (Sec. II A). Also, the theoretical development of the PSRO is discussed (Sec. II B) and applied to the special case of the harmonic oscillator (Sec. II C). Section III provides the details of the numerical application of the PSRO to both basis sets. Section IV presents the results, followed by concluding remarks (Sec. V) of all the data presented, and possible future developments.

II. THEORETICAL BACKGROUND

A. Weyl-Heisenberg wavelets (weylets) and momentum-symmetrized Gaussians (SG's)

A complete analysis of the construction of the weylets and SG's are documented in Refs. [1–3] and Ref. [11], respectively; thus, only the mathematical form of the basis functions will be presented in this paper, along with a brief description. First, the SG's for the single DOF case in arbitrary units where $\hbar=1$ (as will be presumed throughout this paper) have the form

$$\psi_{st}(q) = \left(\frac{4a^2}{\pi}\right)^{1/4} \cos\{ta\sqrt{\pi}[q-(s+1/2)\sqrt{\pi}/a]\} \times e^{-a^2(q-s\sqrt{\pi}/a)^2/2}. \tag{5}$$

The previous index i is replaced with the two indices, s and t, signifying lattice sites $(q_s, \pm p_t)$ where the unsymmetrized pair of phase space Gaussians are centered. The lattice sites are specified by $q_s=(s/a)\sqrt{\pi}$ and $p_t=ta\sqrt{\pi}$, with the parameter a related to the "aspect ratio" of the lattice. Momentum symmetrization requires t to be restricted to positive half integers, i.e., $t=\{0.5,1.5,2.5,\ldots\}$, but $s=\{\ldots,\epsilon-1,\epsilon,\epsilon+1,\ldots\}$ for any real ϵ.

The 1 DOF weylet functions can themselves be expanded into SG's

$$\varphi_{st}(q) = \sum_{m,n=-m_{\max}}^{m_{\max}} (-1)^{(n/2+mt)} c_{mn} \psi_{s+m,t+n}(q), \tag{6}$$

where m and n are even integers and c_{mn} are coefficients listed in Refs. [1,2]. The c_{mn} decay exponentially with respect to $|m|+|n|$; thus, in practice, one can apply a correlated "diamond" summation $\Sigma_{|m|+|n|\le m_{\max}}$ [1,2]. In this paper, the bound on the summation is chosen to be $m_{\max}\le 6$ outside of which all c_{mn} have magnitudes less than 10^{-6}.

For the general f DOF case, the SG's and weylets are products of the 1 DOF functions

$$\psi_{\mathbf{s},\mathbf{t}}(\mathbf{q}) = \prod_{j=1}^{f} \psi_{s_j t_j}(q_j), \tag{7}$$

$$\varphi_{\mathbf{s},\mathbf{t}}(\mathbf{q}) = \prod_{j=1}^{f} \varphi_{s_j t_j}(q_j), \tag{8}$$

where $\mathbf{q}=(q_1,q_2,\ldots,q_f)$, $\mathbf{s}=(s_1,s_2,\ldots,s_f)$, and $\mathbf{t}=(t_1,t_2,\ldots,t_f)$. Each weylet of Eq. (8) is approximately represented by groups of 2^f blocks, with centers at $(q_{s_1},p_{\pm t_1},q_{s_2},p_{\pm t_2},\ldots,q_{s_f},p_{\pm t_f})$, each of volume $(\pi)^f$ [see Fig. 2(a)]. Thus, the set of $2^f N$ blocks $\mathcal{R}'$ has a total volume of $N(2\pi)^f$, and similarly, the set of K target eigenstates $\mathcal{R}$ has a total volume of $K(2\pi)^f$. The SG's of Eq. (7) follow the same design, except that individual functions correspond to phase space "spheres," rather than blocks. The spheres overlap slightly, reflecting nonorthogonality of the SG basis, and also leading to a somewhat lower efficiency of the SG's compared to the weylets.

B. Phase space region operator (PSRO)

In the f DOF case, the action of an arbitrary smooth operator $\hat{A}$ on the basis function $|\vartheta_{\mathbf{s},\mathbf{t}}\rangle$ is

$$(\hat{A}\vartheta_{\mathbf{s},\mathbf{t}})(\mathbf{q}) = \int \langle \mathbf{q}|\hat{A}|\mathbf{q}'\rangle\langle\mathbf{q}'|\vartheta_{\mathbf{s},\mathbf{t}}\rangle d^f q', \tag{9}$$

where $\vartheta_{\mathbf{s},\mathbf{t}}$ can be either the weylets $\varphi_{\mathbf{s},\mathbf{t}}$ or SG's $\psi_{\mathbf{s},\mathbf{t}}$. The term $\langle\mathbf{q}|\hat{A}|\mathbf{q}'\rangle$ in Eq. (9) is known as the "configuration

kernel" of $\hat{A}$, and can be represented by the expression

$$\langle \mathbf{q}|\hat{A}|\mathbf{q}'\rangle = \frac{1}{(2\pi)^f}\int A[(\mathbf{q}+\mathbf{q}')/2,\mathbf{p}]e^{i\mathbf{p}\cdot(\mathbf{q}-\mathbf{q}')}d^f p, \quad (10)$$

where A is the Weyl symbol of $\hat{A}$ [17–20].

The observable of interest is the PSRO, i.e.,

$$A(\mathbf{q},\mathbf{p}) = \rho_K^{\mathrm{QC}}(\mathbf{q},\mathbf{p}) = \Theta[E_{\max} - H(\mathbf{q},\mathbf{p})] = \Theta\left[E_{\max} - \sum_{j=1}^{f} p_j^2/(2m_j) - V(\mathbf{q})\right] \quad (11)$$

for a system with a quantum Hamiltonian in the kinetic-plus-potential form ($\hat{H}=\hat{T}+\hat{V}$) in Cartesian coordinates. Using Eqs. (9) and (10), the PSRO-modified basis functions become

$$(\hat{\rho}_K^{\mathrm{QC}}\vartheta_{\mathbf{s},\mathbf{t}})(\mathbf{q}) = \frac{1}{(2\pi)^f}\int \rho_K^{\mathrm{QC}}[(\mathbf{q}+\mathbf{q}')/2,\mathbf{p}]e^{i\mathbf{p}\cdot(\mathbf{q}-\mathbf{q}')} \times\langle \mathbf{q}'|\vartheta_{\mathbf{s},\mathbf{t}}\rangle d^f p d^f q'. \quad (12)$$

Further simplification is possible for $f=1$ [23,24] as shown below. First, Eq. (11) can be rewritten as

$$\rho_K^{\mathrm{QC}}(q,p) = \begin{cases} 1, & x_{\min} \le q \le x_{\max} \quad \text{and} \quad -p_{\max}(q) \le p \le p_{\max}(q), \\ 0, & \text{otherwise}, \end{cases} \quad (13)$$

where $p_{\max}(q)=\sqrt{2m[E_{\max}-V(q)]}$. Plugging Eq. (13) into Eq. (10), the 1 DOF configuration kernel of the PSRO can be reduced to

$$\langle q|\hat{\rho}_K^{\mathrm{QC}}|q'\rangle = \begin{cases} \dfrac{\sin\left[(q-q')p_{\max}\left(\dfrac{q+q'}{2}\right)\right]}{\pi(q-q')}, & 2x_{\min} \le (q+q') \le 2x_{\max}, \\ 0, & \text{otherwise}. \end{cases} \quad (14)$$

Finally, placing Eq. (14) into Eq. (9), the 1 DOF version of Eq. (12) simplifies to

$$(\hat{\rho}_K^{\mathrm{QC}}\vartheta_{st})(q) = \int_{2x_{\min}-q}^{2x_{\max}-q} \frac{\sin\left[(q-q')p_{\max}\left(\dfrac{q+q'}{2}\right)\right]}{\pi(q-q')}\vartheta_{st}(q')dq'. \quad (15)$$

C. PSRO for the harmonic oscillator (HO)

Consider the multidimensional isotropic HO, where the masses and frequencies are all equal to unity in the previously defined arbitrary units, i.e., $m_j=\omega_j=1$ for $j=1,\ldots,f$ so that $\hat{H}(\hat{\mathbf{q}},\hat{\mathbf{p}})=(1/2)\Sigma_{j=1}^f(\hat{p}_j^2+\hat{q}_j^2)$. The spherical symmetry of this system renders an exact analytical solution of Eq. (12) possible. The QC phase space region $\mathcal{R}=\{(\mathbf{q},\mathbf{p})|0 \le \Sigma_{j=1}^f[p_j^2+q_j^2] \le 2E_{\max}\}$ [where $\rho_K^{\mathrm{QC}}(q,p)=1$] is a $2f$-dimensional hypersphere centered at the phase space origin.

The operator $\hat{\rho}_K^{\mathrm{QC}}$ can always be written in the form

$$\hat{\rho}_K^{\mathrm{QC}} = \sum_i w_i|\Phi_i\rangle\langle\Phi_i|, \quad (16)$$

where w_i are the eigenvalues of $\hat{\rho}_K^{\mathrm{QC}}$ and $|\Phi_i\rangle$ the corresponding eigenfunctions. We then have

$$(\hat{\rho}_K^{\mathrm{QC}}\vartheta_{\mathbf{s},\mathbf{t}})(\mathbf{q}) = \sum_i w_i\langle\Phi_i|\vartheta_{\mathbf{s},\mathbf{t}}\rangle\Phi_i(\mathbf{q}). \quad (17)$$

For the isotropic HO system, the w_i's and corresponding $|\Phi_i\rangle$'s are known analytically, as are the overlaps $\langle\Phi_i|\vartheta_{\mathbf{s},\mathbf{t}}\rangle$.

As shown in Refs. [23,24], the eigenfunctions of $\hat{\rho}_K^{\mathrm{QC}}$ are also those of $\hat{\rho}_K$, i.e., the HO eigenstates

$$|\Phi_i\rangle = |\mathbf{n}\rangle = |n_1\rangle\otimes|n_2\rangle\otimes\cdots\otimes|n_f\rangle, \quad (18)$$

where n_j is a nonnegative integer representing the quantum excitation of the jth DOF of the HO. The eigenvalues can be determined by

$$w_{\mathbf{n}}(E_{\max}) = \langle\mathbf{n}|\hat{\rho}_K^{\mathrm{QC}}|\mathbf{n}\rangle. \quad (19)$$

Using the Wigner-Weyl formalism, Eq. (19) becomes

$$w_{\mathbf{n}}(E_{\max}) = \int \rho_K^{\mathrm{QC}}(\mathbf{q},\mathbf{p})\mathcal{W}_{\mathbf{n}}(\mathbf{q},\mathbf{p})d^f q d^f p = \int_{\mathcal{R}} \mathcal{W}_{\mathbf{n}}(\mathbf{q},\mathbf{p})d^f q d^f p, \quad (20)$$

where $\mathcal{W}_{\mathbf{n}}(\mathbf{q},\mathbf{p})$ represents the Wigner probability distribution function [17–20] of the pure state density operator of each HO eigenfunction, i.e., $|\mathbf{n}\rangle\langle\mathbf{n}|$. The analytical expression is

$$\mathcal{W}_{\mathbf{n}}(\mathbf{q},\mathbf{p}) = \prod_{j=1}^{f} \mathcal{W}_{n_j}(q_j,p_j), \tag{21}$$

where

$$\mathcal{W}_{n_j}(q_j,p_j) = \frac{(-1)^{n_j}}{\pi} L_{n_j}[2(q_j^2+p_j^2)]e^{-(q_j^2+p_j^2)} \tag{22}$$

and L_{n_j} is a Laguerre polynomial of degree n_j.

The above equations imply that the eigenvalues $w_{\mathbf{n}}(E_{\max})$ depend only upon $n_S=\Sigma_{j=1}^{f} n_j$ instead of $\mathbf{n}$ itself, i.e., $w_{\mathbf{n}}(E_{\max})=w_{n_S}(E_{\max})$ which is proven in Refs. [23,24]. Upon integration of Eq. (20), a recurrence relationship can be derived [24]:

$$w_{n_S+1}(E_{\max}) - w_{n_S}(E_{\max}) = \frac{(-1)^{n_S+1}(n_S)!}{2^{f-1}(n_S+f)!} e^{-2E_{\max}}(4E_{\max})^f L_{n_S}^f(4E_{\max}) \tag{23}$$

and

$$w_0(E_{\max}) = P(f,2E_{\max}), \tag{24}$$

where $L_{n_S}^f$ is the associated Laguerre polynomial and $P(f,2E_{\max})$ is the incomplete gamma function. As shown previously, the radius of the hyperspherical region $\mathcal{R}$ is $\sqrt{2E_{\max}}$. Given that $\mathcal{R}$ has a volume of $K(2\pi)^f$, one can derive a useful direct relation between $E_{\max}$ and K:

$$E_{\max} = (Kf!)^{1/f}. \tag{25}$$

Finally, the PSRO used in the calculation of the K HO eigenvalues and eigenfunctions in the decomposed form of Eq. (16) is

$$\hat{\rho}_K^{\mathrm{QC}} = \sum_{n_S \le n_{\max}} w_{n_S}(E_{\max})|\mathbf{n}\rangle\langle\mathbf{n}|, \tag{26}$$

where the sum above includes all states $|\mathbf{n}\rangle$ that have $n_S \le n_{\max}$. The nonnegative integer parameter $n_{\max}$ is chosen such that a desired level of convergence is achieved in the final calculation.

III. NUMERICAL IMPLEMENTATION

A. Morse oscillator (1 DOF)

For 1 DOF realistic potentials, we resort to explicit numerical integration of Eq. (15). Although the application to large K and N is computationally expensive, the small problem sizes of this study are appropriate as the focus is to determine whether this method can achieve significant increases in efficiency. Future projects may involve the development of new time and memory saving techniques or approximations (similar to Sec. III B) to enhance application of this PSRO method to larger problems.

We choose to examine the Morse oscillator, for which

$$\hat{H}(\hat{q},\hat{p}) = \frac{\hat{p}^2}{2} + D(e^{-2\kappa\hat{q}} - 2e^{-\kappa\hat{q}}). \tag{27}$$

The parameters $D=12.000$ and $\kappa=0.2041241$ are chosen so that $\mathcal{R}$ has a volume of 48π at dissociation energy $E_{\max}=0$, thus signifying that there are 24 bound states ($K=24$). For comparison, the eigenvalues w_i or energy values of the bound states can be analytically determined [26]:

$$w_i = -D + \kappa\sqrt{2D}\left(i-\frac{1}{2}\right) - \frac{\kappa^2}{2}\left(i-\frac{1}{2}\right)^2, \tag{28}$$

where $i=1,\ldots,24$.

The PSRO-modified weylets and SG's are numerically computed using MATHEMATICA. A set of points for q spaced at 0.02 increments between boundaries $X_{\min}^{(1)}$ and $X_{\max}^{(1)}$ are used to define each of the N modified basis functions $\vartheta_{st}^{(1)}(q)$ using Eq. (15). The boundaries $X_{\min}^{(1)}$ and $X_{\max}^{(1)}$ span slightly beyond the PSRO region because each projected function $\vartheta_{st}^{(1)}(q)$ extends outside the $[x_{\min}, x_{\max}]$ range, although the extension does decay rapidly. In practice, $x_{\min}-X_{\min}^{(1)}$ and $X_{\max}^{(1)}-x_{\max}$ are chosen to be approximately between 1 and 2 which allows sufficient convergence of the elements of $\tilde{H}$ and $\tilde{S}$.

For functions resulting from the application of the PSRO operator $p>1$ times $\vartheta_{st}^{(p)}(q)=[(\hat{\rho}_K^{\mathrm{QC}})^p\vartheta_{st}](q)$, one needs to determine beforehand all appropriate boundaries for all modified basis functions from $\vartheta_{st}^{(1)}$ to $\vartheta_{st}^{(p)}$. This is done in a reverse fashion by first choosing sufficient boundaries $X_{\min}^{(p)}$ and $X_{\max}^{(p)}$, for $\vartheta_{st}^{(p)}(q)$, i.e., $x_{\min}-X_{\min}^{(p)}$ and $X_{\max}^{(p)}-x_{\max}$ are between 1 and 2, and then using the following equations for the $1 \le b < p$ limits:

$$X_{\min}^{(b)} = \begin{cases} X_{\min}^{(p)} + (p-b)(x_{\min}-x_{\max}), & (p-b)\ \text{even}, \\ -X_{\max}^{(p)} + (p-b)(x_{\min}-x_{\max}) + x_{\max} + x_{\min}, & (p-b)\ \text{odd} \end{cases} \tag{29}$$

and

$$X_{\max}^{(b)} = \begin{cases} X_{\max}^{(p)} + (p-b)(x_{\max}-x_{\min}), & (p-b)\ \text{even}, \\ -X_{\min}^{(p)} + (p-b)(x_{\max}-x_{\min}) + x_{\max} + x_{\min}, & (p-b)\ \text{odd}. \end{cases} \tag{30}$$

One finds that the functions of lower modification need larger boundaries, i.e., $X_{\min}^{(b)} < X_{\min}^{(b')}$ and $X_{\max}^{(b)} > X_{\max}^{(b')}$ for $b < b'$.

B. Morse/harmonic oscillator (2 DOF)

For systems where $f > 1$, the Eq. (12) integrations are rather costly, even for $f=2$, for which four-dimensional integrals are needed. In such cases however, one may apply a separable PSRO modification to greatly reduce the computational cost. In this section, we apply this idea to the 2 DOF Morse/HO system,

$$\hat{H}(\hat{x}',\hat{y}',\hat{p}_x,\hat{p}_y) = \frac{1}{2}(\hat{p}_x^2 + \hat{p}_y^2) + \frac{(\hat{x}')^2}{2} + D(e^{-2\kappa\hat{y}'} - 2e^{-\kappa\hat{y}'} + 1), \tag{31}$$

which becomes coupled via rotation of the coordinates

$$x = x'\cos 10^{\circ} + y'\sin 10^{\circ} \tag{32}$$

and

$$y = -x'\sin 10^{\circ} + y'\cos 10^{\circ}. \tag{33}$$

Instead of using the $\rho_K^{\mathrm{QC}}(x,y,p_x,p_y)$ PSRO which is coupled, one applies the separable approximation $\rho_{K_x}^{\mathrm{QC}}(x,p_x)\rho_{K_y}^{\mathrm{QC}}(y,p_y)$, where $K_x K_y \geq K$. Since the $\vartheta_{\mathbf{s,t}}$ basis is also separable, one obtains

$$\begin{aligned}(\hat{\rho}_K^{\mathrm{QC}}\vartheta_{\mathbf{s,t}})(x,y) &= \int_{2x_{\min}-x}^{2x_{\max}-x} \frac{\sin\left[(x-x')p_{x_{\max}}\left(\frac{x+x'}{2}\right)\right]}{\pi(x-x')}\vartheta_{s_x t_x}(x')dx' \\ &\times \int_{2y_{\min}-y}^{2y_{\max}-y} \frac{\sin\left[(y-y')p_{y_{\max}}\left(\frac{y+y'}{2}\right)\right]}{\pi(y-y')}\vartheta_{s_y t_y}(y')dy' \\ &= \vartheta_{s_x t_x}^{(1)}(x)\,\vartheta_{s_y t_y}^{(1)}(y),\end{aligned} \tag{34}$$

where $p_{x_{\max}}(x) = \sqrt{2[E_{\max} - V_x(x)]}$ and $p_{y_{\max}}(y) = \sqrt{2[E_{\max} - V_y(y)]}$. Any of a number of techniques may be used to obtain suitable 1 DOF marginal potentials (V_x and V_y), with the primary criterion being that $\rho_{K_x}^{\mathrm{QC}}\rho_{K_y}^{\mathrm{QC}}$ resemble ρ_K^{QC} as closely as possible. For this paper, we use the method of Ref. [27].

The marginal potentials V_x and V_y resulting from the optimization can be found by simply minimizing the original potential with respect to y and x, respectively [28,29], i.e.,

$$V_x(x) = \min[V(x,y)]_y \tag{35}$$

and

$$V_y(y) = \min[V(x,y)]_x. \tag{36}$$

No adjustments need to be made for the above equations, since $\min[V(x,y)] = 0$.

The classically allowed region corresponding to the separable PSRO has a "cylindrical" shape composed of the product of 2 two-dimensional phase space regions $\mathcal{R}_x \times \mathcal{R}_y$. This region contains "corners" not present in the nonzero region of ρ_K^{QC}. Thus, the separable PSRO is different from, and less effective than $\hat{\rho}_K^{\mathrm{QC}}$, in the sense that it fails to smooth out all of the peripheral lattice states due to the wasted space of the corners.

C. Harmonic oscillator (HO)

For the HO system, one does not need to bother with the numerical integrations needed for the realistic cases presented in Secs. III A and III B. Instead, an analytical representation of Eq. (12), as presented in Sec. II C, can be used; thus, one can avoid the numerical errors coming from the computationally expensive integrations.

Ultimately, we want to represent the HO Hamiltonian in the PSRO-modified SG $|\psi_{\mathbf{s,t}}^{(1)}\rangle$ or weylet $|\varphi_{\mathbf{s,t}}^{(1)}\rangle$ basis. Using Eq. (26) and the eigenvalue relationship $\hat{H}|\mathbf{n}\rangle = (n_S + f/2)|\mathbf{n}\rangle$, the Hamiltonian matrix elements in the modified SG basis are given by

$$\begin{aligned}[\tilde{H}^{\psi^{(1)}}]_{\mathbf{s,t,s',t'}} &= \langle\psi_{\mathbf{s,t}}^{(1)}|\hat{H}|\psi_{\mathbf{s',t'}}^{(1)}\rangle \\ &= \sum_{n_S \leq n_{\max}} [w_{n_S}(E_{\max})]^2 (n_S + f/2) \\ &\times \prod_{j=1}^{f} (\langle\psi_{s_j t_j}|n_j\rangle\langle n_j|\psi_{s'_j t'_j}\rangle).\end{aligned} \tag{37}$$

To solve Eq. (4), we also need the overlap matrix

$$\begin{aligned}[\tilde{S}^{\psi^{(1)}}]_{\mathbf{s,t,s',t'}} &= \langle\psi_{\mathbf{s,t}}^{(1)}|\psi_{\mathbf{s',t'}}^{(1)}\rangle \\ &= \sum_{n_S \leq n_{\max}} [w_{n_S}(E_{\max})]^2 \\ &\times \prod_{j=1}^{f} (\langle\psi_{s_j t_j}|n_j\rangle\langle n_j|\psi_{s'_j t'_j}\rangle).\end{aligned} \tag{38}$$

Similar equations apply for the weylet basis. The overlaps are given explicitly as follows:

$$\langle\psi_{st}|n\rangle = \frac{\pi^{n/2}}{\sqrt{2^{n-1}n!}} e^{-(\pi/4)(s^2+t^2)} \mathrm{Re}[(s+it)^n e^{-i(\pi/2)t(s+1)}] \tag{39}$$

and

$$\langle\varphi_{st}|n\rangle = \sum_{m,n=-m_{\max}}^{m_{\max}} (-1)^{(n/2+mt)} c_{mn}\langle\psi_{st}|n\rangle. \tag{40}$$

In the above expressions, we have chosen the parameters $a = 1$ and $\epsilon = 1/2$. The generalization for $|\psi_{\mathbf{s,t}}^{(p)}\rangle$ is obtained by replacing $[w_{n_S}(E_{\max})]^2$ with $[w_{n_S}(E_{\max})]^{2p}$ in Eqs. (37) and (38).

IV. RESULTS

A. Morse oscillator (1 DOF)

For the 1 DOF Morse oscillator system, we optimized our calculations for the lowest $K=6$ eigenstates. These are suffi-

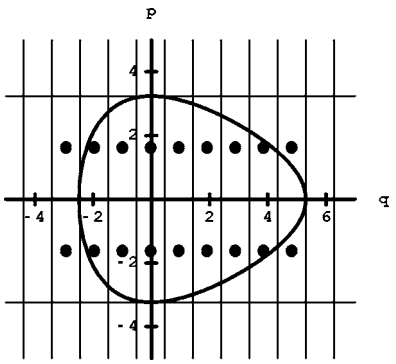

FIG. 3. Classically allowed region for the 1 DOF weylets and Morse PSRO. The egg-shaped region $\mathcal{R}$ represents the 1 DOF Morse system at $E_{\max}=-6.7500$. There are $K=6$ eigenstates at that energy (area inside is 12π). Filled circles indicate the centers of the $N=9$ basis functions used for the calculation of the six corresponding eigenvalues (Table I).

ciently far below dissociation that the QC eigenstate region $\mathcal{R}$ ($E_{\max}=-6.7500$) is convex, suitable for the SG's and weylets, yet the last few eigenstates are high enough to clearly exhibit anharmonic behavior (note the shape of $\mathcal{R}$ in Fig. 3). The $N=9$ basis functions are chosen to sufficiently cover $\mathcal{R}$ and are each modified by the PSRO $\hat{\rho}_6^{\mathrm{QC}}$. In practice, a suitable basis size N depends strongly on K. If N is insufficiently larger than K, then the PSRO is ineffective at computing all K desired states to sufficient accuracy. On the other hand, if N is too large, then the overlap matrix $\tilde{S}$ is ill conditioned (eigenvalues of $\tilde{S}$ are too small) preventing generalized eigenvalue routines from solving Eq. (4).

The weylet basis functions were chosen as in Fig. 3. The selection is very similar to what would be obtained via the phase space truncation criterion used in Secs. IV C and IV B. We chose $a=1.8282$ such that the heights of the lattice cells equal the maximum extent of $\mathcal{R}$ in the positive and negative momentum direction. Based on previous work [11], this determination of a yields reasonable efficiency (in general, the efficiency is not sensitively dependent on a unless the basis size is very small). Also, the position (horizontal) shift of the rectangles are adjusted ($\epsilon=-0.0273$) so that the right edge of the block furthest along the position axis (in the positive direction) corresponds to the right boundary $x_{\max}=5.3058$ of $\mathcal{R}$. The left boundary $x_{\min}=-2.4871$ of $\mathcal{R}$ extends slightly further than one basis function; thus, we added a ninth basis function on the negative side for sufficient coverage.

TABLE I. The absolute differences between computed and analytical [Eq. (28)] values for the lowest nine energy levels of the 1 DOF Morse potential, using various basis sets of $N=9$ functions in each case.

State index	$\lvert\varphi_{st}\rangle$	$\lvert\varphi_{st}^{(1)}\rangle$	$\lvert\varphi_{st}^{(2)}\rangle$	$\lvert\psi_{st}\rangle$	$\lvert\psi_{st}^{(1)}\rangle$	$\lvert\psi_{st}^{(2)}\rangle$
1	0.08778	0.00026	0.00002	0.10436	0.00032	0.00002
2	0.21867	0.00405	0.00004	0.23072	0.00404	0.00003
3	0.34136	0.00313	0.00019	0.35087	0.00369	0.00018
4	0.46269	0.00634	0.00039	0.46868	0.00609	0.00040
5	0.60569	0.02051	0.00028	0.62050	0.02014	0.00029
6	0.38179	0.01320	0.00008	0.39710	0.01495	0.00011
7	0.58765	0.14343	0.08323	0.57373	0.14473	0.08307
8	1.80886	1.64599	1.13088	1.74577	1.66911	1.12617
9	2.62491	3.23755	3.07434	2.66852	3.12843	3.06419

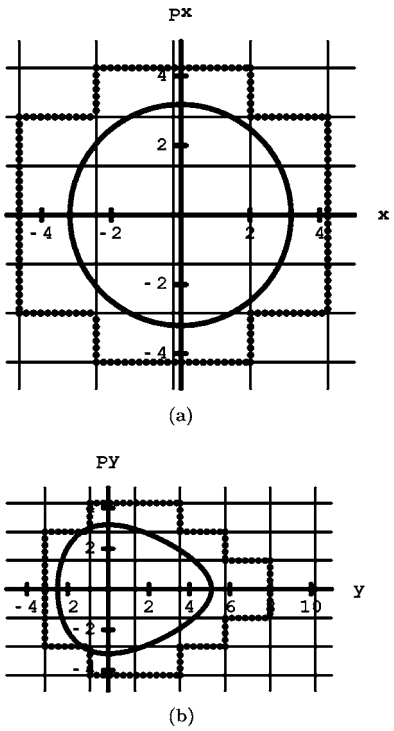

FIG. 4. Classically allowed region of the separable PSRO for the 2 DOF Morse/HO system. $\mathcal{R}_x$ and $\mathcal{R}_y$ are shown in parts (a) and (b), respectively, as the inner "solid" curve. $\mathcal{R}_x'$ and $\mathcal{R}_y'$, reflective of the basis set ($N=49$) of SG's, are also shown in parts (a) and (b) outlined by the "dotted" lines.

We considered both the SG's and weylets as basis sets, as well as their PSRO-modified versions, up to $p=3$. The triple modified functions $\vartheta_{st}^{(3)}(q)$ lie between chosen boundaries of $X_{\min}^{(3)}=-4$ and $X_{\max}^{(3)}=7$, sufficiently outside of the PSRO bounds $x_{\min}$ and $x_{\max}$. By Eqs. (29) and (30), the bounds of the $b<p$ functions are $X_{\min}^{(2)}=-11.9743$, $X_{\min}^{(1)}=-19.5859$, $X_{\max}^{(2)}=14.6116$, and $X_{\max}^{(1)}=22.5859$. We report in Table I the absolute errors between the calculated and analytical values for all basis set types except for the $p=3$ case, since these show no improvement over the $p=2$ case.

In both the weylet and SG case, the greatest reduction in the absolute error from the unmodified to the modified case occurs in the lowest eigenstates. For example, a near-4-order-of-magnitude improvement in accuracy is shown for the lowest two eigenvalues of the $p=2$ weylets $\lvert\varphi_{st}^{(2)}\rangle$ and SG's $\lvert\psi_{st}^{(2)}\rangle$ relative to the corresponding unmodified basis sets $\lvert\varphi_{st}\rangle$ and $\lvert\psi_{st}\rangle$. The $\lvert\varphi_{st}^{(1)}\rangle$ and $\lvert\psi_{st}^{(1)}\rangle$ sets show accuracy improvements ranging from 1–3 orders of magnitude for all six targeted eigenvalues. In general, both of the SG's and weylets follow the same pattern vis-à-vis the PSRO modification, and exhibit comparable accuracies for the same p value, even in the unmodified case $p=0$. This advocates

TABLE II. Lowest 20 eigenvalues of the 2 DOF Morse/HO system. Analytical eigenvalues are in column 2, whereas columns 3 and 4 present absolute differences between computed (with indicated basis of $N=49$ functions) and analytical values.

State index	exact	$\|\psi_{\mathbf{s,t}}\rangle$	$\|\psi^{(1)}_{\mathbf{s,t}}\rangle$
1	0.99479	0.11071	0.00723
2	1.95312	0.16049	0.00792
3	1.99479	0.13723	0.01968
4	2.86979	0.18210	0.01107
5	2.95312	0.15255	0.01331
6	2.99479	0.28710	0.04711
7	3.74479	0.10967	0.00307
8	3.86979	0.26459	0.02560
9	3.95312	0.22814	0.00793
10	3.99479	0.51273	0.13002
11	4.57812	0.27680	0.02238
12	4.74479	0.23347	0.01640
13	4.86979	0.49817	0.04803
14	4.95312	0.46867	0.06308
15	4.99479	0.78611	0.36803
16	5.36979	0.61201	0.04981
17	5.57812	0.49562	0.04201
18	5.74479	0.46122	0.04282
19	5.86979	0.60898	0.09321
20	5.95312	0.78684	0.33679

strongly in favor of using SG basis functions for practical applications. The main conclusion, though, is that PSRO modification is extremely effective for either basis set, with the largest relative error for the targeted $K=6$ energies being only around 3×10^{-5} for $p=2$. Table I also indicates errors for the remaining $N-K=3$ eigenvalues, which show only small improvements and sometimes loss of accuracy by the PSRO modification, thus demonstrating the ability of the method to single out just the desired K eigenvalues from the others.

B. Morse/harmonic oscillator (2 DOF)

We developed a separable PSRO that corresponds to a product region $\mathcal{R}_x\times\mathcal{R}_y$, where both components are projected regions onto the (x,p_x) and (y,p_y) axes [27], respectively, of $\mathcal{R}$, the classically allowed region of the lowest $K=14$ eigenstates ($E_{\max}=5.0700$) of the 2 DOF Morse/HO system. We applied the PSRO to each of the SG basis functions ($N=49$) selected by the basis truncation criterion $H(q_s,p_t)\leq E_{\text{cut}}=9.0000$ [1–3]. In parts (a) and (b) of Fig. 4, the inner curves (solid line) denote $\mathcal{R}_x$ and $\mathcal{R}_y$, respectively, with boundaries of $x_{\min}=-3.1911$ and $x_{\max}=3.1797$ for the former and $y_{\min}=-2.4942$ and $y_{\max}=5.0820$ for the latter. The projections of $\mathcal{R}'$, the classically allowed region of the SG basis set (actually, more reflective of the weylets), are highlighted by the dotted lines and, in a fashion similar to PSRO regions, are labeled as $\mathcal{R}'_x$ and $\mathcal{R}'_y$. The parameters of the SG basis set were chosen to produce optimal computed eigenvalues for the unmodified basis set and are listed as follows: $a_x=a_y=0.7979$, $\epsilon_x=0.4064$, and $\epsilon_y=0.0926$.

TABLE III. Results for the 1 DOF isotropic HO system computed using six different basis sets. The values under the different basis columns indicate the number of eigenvalues computed to relative accuracy indicated in column 3.

E_{cut}	N	accuracy	$\|\varphi_{st}\rangle$	$\|\varphi^{(1)}_{st}\rangle$	$\|\varphi^{(2)}_{st}\rangle$	$\|\psi_{st}\rangle$	$\|\psi^{(1)}_{st}\rangle$	$\|\psi^{(2)}_{st}\rangle$
4.0	6	2×10^{-2}	2	5	6	2	6	6
		2×10^{-3}	0	3	5	0	3	5
		2×10^{-4}	0	1	2	0	0	3
		2×10^{-5}	0	0	1	0	0	1
110.0	108	2×10^{-2}	84	97	104	81	97	104
		2×10^{-4}	53	75	88	48	54	83
		2×10^{-6}	31	47	50	22	37	47
		2×10^{-8}	17	20	29	7	18	20
		2×10^{-10}	4	6	13	0	3	5
		2×10^{-12}	0	1	2	0	0	0
177.0	180	2×10^{-2}	144	157	172	139	156	172
		2×10^{-4}	105	118	131	97	108	121
		2×10^{-6}	74	93	98	61	83	92
		2×10^{-8}	52	60	75	35	54	58
		2×10^{-10}	28	35	53	17	28	36
		2×10^{-12}	6	24	27	7	13	21
		2×10^{-14}	0	7	7	1	5	5

The analytical eigenvalues of the Morse/harmonic oscillator (column 2 of Table II) are equal to the sum of the Morse [Eq. (28)] and 1 DOF harmonic eigenvalues, exactly like the uncoupled case [Eq. (31)], since the coupling is only due to a rotation on the (x,y) plane. Improvements up to two orders of magnitude are shown for the modified versus unmodified case. Note that there is not a clear divorcing of the first 14 and the remaining 6 reported in Table II, as there is in Table I; although, the accuracy improvements diminish rapidly beyond the $K=14$ cutoff. This behavior is due to the artificial separability used in the 2 DOF PSRO. The method is nevertheless quite effective at improving the accuracy of the desired eigenvalues.

C. Harmonic oscillator (HO)

The isotropic HO up to 4 DOF's was solved using six different basis sets ($a=1$): $|\varphi_{\mathbf{s,t}}\rangle$, $|\varphi^{(1)}_{\mathbf{s,t}}\rangle$, $|\varphi^{(2)}_{\mathbf{s,t}}\rangle$, $|\psi_{\mathbf{s,t}}\rangle$, $|\psi^{(1)}_{\mathbf{s,t}}\rangle$, and $|\psi^{(2)}_{\mathbf{s,t}}\rangle$ (Tables III–VI). In all cases, the basis truncation criterion $H(q_s,p_t)\leq E_{\text{cut}}$ [1–3] was used to obtain a representational basis of size N. We also chose $K=N$, i.e., we set the volume of the PSRO region $\mathcal{R}$ to equal that of the basis region $\mathcal{R}'$ [Fig. 2(a)].

In Fig. 1, we can see, pictorially, how the PSRO affects the weylets in the 1 DOF case. Part (a) shows the Wigner probability distribution function of the projection operator containing the lowest 6 HO eigenstates. Part (b) gives the

TABLE IV. Number of accurately computed eigenvalues for the 2 DOF isotropic HO system using six different basis sets (consult Table III for further details).

E_{cut}	N	accuracy	$\lvert\varphi_{\mathbf{s,t}}\rangle$	$\lvert\varphi^{(1)}_{\mathbf{s,t}}\rangle$	$\lvert\varphi^{(2)}_{\mathbf{s,t}}\rangle$	$\lvert\psi_{\mathbf{s,t}}\rangle$	$\lvert\psi^{(1)}_{\mathbf{s,t}}\rangle$	$\lvert\psi^{(2)}_{\mathbf{s,t}}\rangle$
20.0	176	2×10^{-2}	73	139	154	71	140	154
		2×10^{-3}	31	69	113	16	67	111
		2×10^{-4}	3	29	49	0	8	42
		2×10^{-5}	0	0	8	0	0	5
70.0	2340	2×10^{-2}	1375	1900	2097	1341	1899	2099
		2×10^{-4}	510	882	1133	363	575	919
		2×10^{-6}	32	279	355	37	146	223
		2×10^{-8}	1	23	45	1	6	11
		2×10^{-10}	0	0	1	0	0	0
140.0	9956	2×10^{-2}	6730	8167	8826	6557	8153	8818
		2×10^{-4}	3597	4968	5740	2966	3748	4788
		2×10^{-6}	1906	2563	2874	1097	1806	2279
		2×10^{-8}	712	913	1218	280	672	773
		2×10^{-10}	120	235	416	46	94	134
		2×10^{-12}	4	29	56	0	0	1
		2×10^{-14}	0	0	1	0	0	0
205.0	20 864	2×10^{-2}	14 917	17 406	18 661	14 569	17 356	18 647
		2×10^{-4}	9037	11 440	13 053	7808	9221	11 103
		2×10^{-6}	5416	7043	7710	3679	5260	6170
		2×10^{-8}	2738	3320	3959	1500	2618	2990
		2×10^{-10}	998	1424	1844	620	881	1129
		2×10^{-12}	47	637	757	81	142	305
		2×10^{-14}	0	15	24	0	3	5
		2×10^{-16}	0	2	2	0	0	1

same setup for the 6 weylets chosen as a basis to solve the HO Hamiltonian [the QC region of (b) is the collective region of blocks in Fig. 2(a)], and part (c) represents the same weylet set under a single PSRO modification. The modified weylets show concentric ring-like features much like the HO eigenstates resulting in a considerable amount of improvement in efficiency over the unmodified set (Table III)—although, one can still observe residual rectilinear weylet features in the slight boxlike cornering of the rings.

The analytical eigenvalues of the isotropic HO are $(n_S + f/2)$, with degeneracy

$$\deg(n_S,f) = \begin{pmatrix} n_S + f - 1 \\ f - 1 \end{pmatrix} \tag{41}$$

for $f > 1$ (the eigenvalues are of course nondegenerate for $f = 1$). They are compared to the actual calculated eigenvalues using the different basis sets, and Tables III–VII report how many of the computed values fall within relative accuracies of 2×10^{-2}, 2×10^{-3}, 2×10^{-4}, and so on [which correspond to error tolerances of $(0.2)f$, $(0.02)f$, $(0.002)f$, …, respectively [3]]. Table VII stands apart from the other HO tables in that it reports the effects of basis set efficiencies as one

TABLE V. Number of accurately computed eigenvalues for the 3 DOF isotropic HO system using six different basis sets (consult Table III for further details).

E_{cut}	N	accuracy	$\lvert\varphi_{\mathbf{s,t}}\rangle$	$\lvert\varphi^{(1)}_{\mathbf{s,t}}\rangle$	$\lvert\varphi^{(2)}_{\mathbf{s,t}}\rangle$	$\lvert\psi_{\mathbf{s,t}}\rangle$	$\lvert\psi^{(1)}_{\mathbf{s,t}}\rangle$	$\lvert\psi^{(2)}_{\mathbf{s,t}}\rangle$
9.0	176	2×10^{-2}	50	137	141	50	140	141
		2×10^{-3}	1	22	49	0	25	52
		2×10^{-4}	0	3	19	0	3	19
21.5	1928	2×10^{-2}	661	1443	1595	622	1445	1594
		2×10^{-3}	185	482	851	89	452	851
		2×10^{-4}	18	118	256	4	35	171
		2×10^{-5}	1	1	20	0	0	3
40.0	9552	2×10^{-2}	4067	7188	7985	3884	7195	7994
		2×10^{-3}	1728	3095	4446	1122	2934	4355
		2×10^{-4}	517	1295	1905	211	568	1317
		2×10^{-5}	119	267	502	28	103	196
		2×10^{-6}	18	66	105	0	12	29
		2×10^{-7}	0	9	17	0	0	1
		2×10^{-8}	0	0	1	0	0	0

TABLE VI. Number of accurately computed eigenvalues for the 4 DOF isotropic HO system using six different basis sets (consult Table III for further details).

E_{cut}	N	accuracy	$\lvert\varphi_{\mathbf{s,t}}\rangle$	$\lvert\varphi^{(1)}_{\mathbf{s,t}}\rangle$	$\lvert\varphi^{(2)}_{\mathbf{s,t}}\rangle$	$\lvert\psi_{\mathbf{s,t}}\rangle$	$\lvert\psi^{(1)}_{\mathbf{s,t}}\rangle$	$\lvert\psi^{(2)}_{\mathbf{s,t}}\rangle$
6.5	144	2×10^{-2}	15	90	90	15	90	90
		2×10^{-3}	0	5	14	0	5	20
		2×10^{-4}	0	0	4	0	0	4
13.0	1616	2×10^{-2}	372	1174	1212	355	1168	1212
		2×10^{-3}	25	118	388	5	99	411
		2×10^{-4}	0	1	16	0	0	11
22.0	12 720	2×10^{-2}	3679	9283	10 098	3473	9300	10 090
		2×10^{-3}	632	1938	4098	282	1827	4045
		2×10^{-4}	45	350	637	1	46	311
		2×10^{-5}	0	1	1	0	0	0

TABLE VII. Number of accurately computed eigenvalues for the 2 DOF isotropic HO system at $E_{\text{cut}}=70.0$ ($N=2340$) using modified weylet basis with the PSRO applied from 3 to 11 times. Beyond $p=11$, numerical difficulties arise in the diagonalization of the Hamiltonian matrix.

accuracy	3	5	7	9	11
2×10^{-2}	2161	2204	2218	2226	2242
2×10^{-3}	1772	1933	2039	2088	2121
2×10^{-4}	1343	1633	1778	1870	1956
2×10^{-5}	792	1142	1439	1610	1719
2×10^{-6}	441	690	986	1218	1385
2×10^{-7}	246	392	627	835	1056
2×10^{-8}	71	142	302	507	689
2×10^{-9}	17	28	106	256	417
2×10^{-10}	1	4	24	86	223
2×10^{-11}	0	0	1	28	92

increases p, the power of the PSRO operator.

For this analysis, we define the efficiency to be L/N, where L is the number of eigenvalues actually computed to a certain relative accuracy as opposed to the number of targeted eigenstates K used to defined the PSRO ($K=N$ for the HO case). This efficiency for $f=2$ at 2×10^{-4} relative accuracy is plotted against N in Fig. 5 which demonstrates similar efficiency curves (apart from a shift) for all six basis types. Although $\lvert\varphi^{(p)}_{\mathbf{s,t}}\rangle$ is now substantially more efficient than $\lvert\psi^{(p)}_{\mathbf{s,t}}\rangle$, the effect is still no greater than that of the PSRO modification itself, in that $\lvert\varphi_{\mathbf{s,t}}\rangle$ and $\lvert\psi^{(1)}_{\mathbf{s,t}}\rangle$ are comparable. Note the large increase in efficiency from $N=176$ to 2340; this "efficiency cliff" [3] shifts to the right with increasing dimensionality, and is the leading cause of accuracy restrictions on weylet calculations at higher dimensionalities. The fact that the PSRO improvements are comparable on and off the cliff is thus highly encouraging.

Figure 6 clearly shows that the efficiencies (2×10^{-2} accuracy) of all basis types do not decay exponentially as the DOF's increase ($N\approx10\,000$ is held constant). The results of the weylets and the SG's are very similar in these plots: the weylets are slightly better than the SG's in the unmodified case, and for both the single and double PSRO-modified sets, the results are essentially identical (modified weylets are not shown). These similarities are only true at the 2×10^{-2} accuracy, whereas higher accuracies display significant improvement of the weylets over SG's, as shown in the previous analysis. The most important result is that the efficiency of the modified functions decreases significantly slower than the unmodified with increasing f; thus, the benefits of PSRO modifications are expected to be substantially greater at larger dimensionality.

In general, the PSRO projection operator significantly improves the efficiency of both the SG's and weylets as demonstrated by all tables and plots. Also, the modifications produce bases that allow for the calculation of a large number of

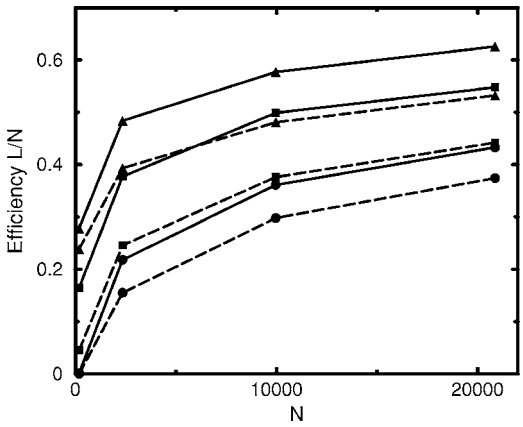

FIG. 5. Efficiency versus N for the 2 DOF HO at 2×10^{-4} relative accuracy (Table IV). The "solid" lines correspond to the weylets either unmodified (circles), single PSRO-modified (squares), or double PSRO-modified (triangles). The "dashed" lines represent the SG's.

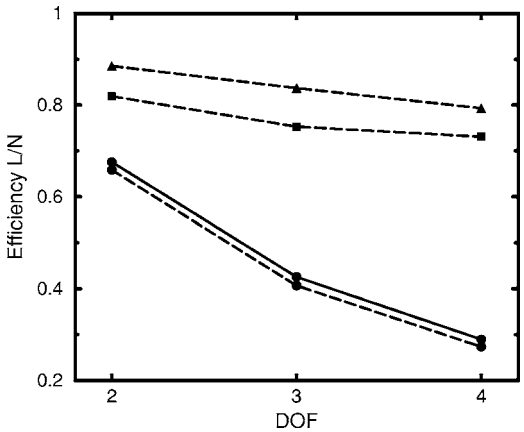

FIG. 6. Efficiency versus DOF's at $N\approx10\,000$ held constant for the HO system. The three data points for each line, starting from the left 2 DOF point, represent basis sizes of $N=9956$, 9552, and 12 720, with L at relative accuracy of 2×10^{-2}. The labels for the plots are the same as that in Fig. 5. Only the SG's are plotted for the modified cases since they are very similar to the weylets.

eigenvalues at extremely high accuracies, otherwise not attainable. For example, in the 2 DOF case (Table IV), there are $L=757$ ($N=20\,864$) eigenvalues that fall within the relative accuracy of 2×10^{-12} using the $|\varphi^{(2)}_{\mathbf{s,t}}\rangle$ basis. Even the less efficient basis $|\psi^{(2)}_{\mathbf{s,t}}\rangle$ is impressive at $L=305$ at similar conditions. A particularly surprising result is to be found in Table VII, for which over 1000 eigenvalues are computed to 2×10^{-7} accuracy, using the $|\varphi^{(11)}_{\mathbf{s,t}}\rangle$ basis of only $N=2340$ functions. Thus, the PSRO to the 11 power is very close to the actual projection operator $\hat{\rho}_K$.

V. CONCLUSION

In this paper, we focus on the combination of two strategies for improving the efficiency of basis sets when solving the nuclear time-independent Schrödinger equation for molecular systems: (1) at the collective level, customization of the basis set as a whole and (2) at the individual level, customization of each basis function. The former refers to the phase space truncation scheme [1–3] which selects the weylet or SG basis for optimal efficiency. The latter is the PSRO modification, which is a completely new approach introduced in this paper, where the PSRO is an easily attainable approximation [23,24] to the actual system's eigenstate projection operator $\hat{\rho}_K$. Remarkable efficiencies can be achieved by using both methods in conjunction, i.e., applying the PSRO to each of the functions in the phase space truncated weylet or SG basis set, which achieves efficiencies that far surpass that attained by using (1) alone—especially useful in cases where the latter is limited in accuracy, or when K and N are small.

For realistic 1 DOF systems, we have shown that one can successfully apply the PSRO to either a suitable weylet or SG basis via numerical integration to produce a new and more efficient basis. The diagonalization of the Hamiltonian matrix in the new basis representation leads to large improvements in energy eigenvalue accuracy when compared to the unmodified basis sets. In the 1 DOF case, the numerical PSRO application is not computationally expensive; however, the same computations do become a serious problem at larger dimensionalities. The favorable symmetry of the model HO system allows the analyses of higher DOF calculations, which would otherwise not be possible, since the Hamiltonian and overlap matrix elements in the modified (as well as unmodified) basis representations can be found by analytical expressions. The purpose of the previous exercise is to clearly show that efficiency and accuracy improvements become even better as one increases f. This promising result provides motivation to explore algorithms that would reduce computations involving real systems of multiple DOF's, for example, the separable PSRO of Sec. III B. For large basis sizes N and number of PSRO modifications p, the computational effort becomes expensive, but is clearly worth exploring further. One idea for possible future work involves the application of Monte Carlo integration methods to the phase space integration in Eq. (12).

ACKNOWLEDGMENTS

This work was supported by awards from The Welch Foundation (D-1523), Research Corporation, and the Office of Advanced Scientific Computing Research, Mathematical, Information, and Computational Sciences Division of the U.S. Department of Energy, under Contract No. DE-FG03-02ER25534. One of the authors (B.P.) gratefully acknowledges Cosmas Zachos for useful discussions.

[1] B. Poirier, J. Theor. Comput. Chem. **2**, 65 (2003).
[2] B. Poirier and A. Salam, J. Chem. Phys. **121**, 1690 (2004).
[3] B. Poirier and A. Salam, J. Chem. Phys. **121**, 1704 (2004).
[4] J. M. Bowman, Comput. Phys. Commun. **51**, 225 (1988).
[5] Z. Bačić and J. C. Light, Annu. Rev. Phys. Chem. **40**, 469 (1989).
[6] G. C. Carney, L. L. Sprandel, and C. W. Kern, Adv. Chem. Phys. **37**, 305 (1978).
[7] J. M. Bowman, J. Chem. Phys. **68**, 608 (1978).
[8] J. M. Bowman, Acc. Chem. Res. **19**, 202 (1986).
[9] B. Poirier and J. C. Light, J. Chem. Phys. **111**, 4869 (1999).
[10] B. Poirier and J. C. Light, J. Chem. Phys. **113**, 211 (2000).
[11] R. Lombardini and B. Poirier, J. Chem. Phys. **124**, 144107 (2006).
[12] J. Montgomery and B. Poirier, J. Chem. Phys. **119**, 6609 (2003).
[13] R. Balian, C. R. Seances Acad. Sci., Ser. 2 **292**, 1357 (1981).
[14] F. Low, *Complete Sets of Wave-Packets* (World Scientific, Singapore, 1985), pp. 17–22.
[15] K. G. Wilson (unpublished).
[16] I. Daubechies, S. Jaffard, and J. Journé, SIAM J. Math. Anal. **22**, 554 (1991).
[17] H. Weyl, Z. Phys. **46**, 1 (1928).
[18] E. Wigner, Phys. Rev. **40**, 749 (1932).
[19] J. E. Moyal, Proc. Cambridge Philos. Soc. **45**, 99 (1949).
[20] M. Hillery, R. F. O'Connell, M. O. Scully, and E. P. Wigner, Phys. Rep. **106**, 121 (1984).
[21] B. Poirier, Found. Phys. **30**, 1191 (2000).
[22] P.-O. Löwdin, Adv. Phys. **5**, 1 (1956).
[23] A. J. Bracken, H.-D. Doebner, and J. G. Wood, Phys. Rev. Lett. **83**, 3758 (1999).
[24] J. G. Wood, Ph.D. thesis, University of Queensland, St. Lucia 4072, Australia, 2003.
[25] M. J. Davis and E. J. Heller, J. Chem. Phys. **71**, 3383 (1979).
[26] S. Flugge, *Practical Quantum Mechanics* (Springer-Verlag, New York, 1971), Vol. 1, p. 94.
[27] W. Bian and B. Poirier, J. Theor. Comput. Chem. **2**, 583 (2003).
[28] H. Chen, S. Liu, and J. C. Light, J. Chem. Phys. **110**, 168 (1999).
[29] Z. Bačić and J. C. Light, J. Chem. Phys. **86**, 3065 (1987).